



## Abstract

The 8 ka B.P. (6050 BCE) pantelleritic obsidian flow on Mayor Island, Bay of Plenty, New Zealand, has been investigated using 30 samples from two sites. Due to a very high paramagnetic/ferromagnetic ratio it was not possible to determine the remanence carriers. This is despite the fact that the samples were studied intensively at low, room and high temperatures. We infer that a stable remanence within the samples is carried by single- or close to single-domain particles. Experiments to determine the anisotropy of thermoremanence tensor and the dependency on cooling rate were hampered due to alteration resulting from the repeated heating of the samples to temperatures just below the glass transition. Nonetheless, a well-defined mean paleointensity of  $57.0 \pm 1.0 \mu\text{T}$ , based on individual high quality paleointensity determinations, was obtained. This field value compares very well to a paleointensity of  $58.1 \pm 2.9 \mu\text{T}$  which Tanaka et al. (2009) obtained for 5500 BCE at a site 100 km distant. Agreement with geomagnetic field models, however, is poor. Thus, gathering more high-quality paleointensity data for the Pacific region and for the Southern Hemisphere in general to better constrain global field models is very important.

## 1 Introduction

The quality of global geomagnetic field models is always restricted by the quality and distribution of the included data. While the quality of paleodirections is assuredly high, paleointensities are thought to be less reliable. During the conduction of paleointensity experiments one must be aware of potential problems such as alteration during geological time or even during the laboratory experiment itself (Valet et al., 1996), anisotropy of thermoremanence (Veitch et al., 1984), magnetic domain state bias (Leonhardt et al., 2004b) and different cooling histories in laboratory and nature (Leonhardt et al., 2006). Especially during the last few years, several studies have tried to deal with these problems and to improve the quality of paleointensity determination either by

SED

3, 679–711, 2011

## Paleointensity on 8 ka New Zealand obsidian

A. Ferk et al.

Title Page

Abstract

Introduction

Conclusions

References

Tables

Figures

◀

▶

◀

▶

Back

Close

Full Screen / Esc

Printer-friendly Version

Interactive Discussion





B.P. (6050 ± 70 BCE; radiocarbon-dated (Buck et al., 1981)) flow studied in this paper predates this last collapse event (6.3 ka (Houghton and Wilson, 1986)). The 8 ka deposit consists of a 1 m thick pumice fall bed that is overlain by a 20 to 70 m thick lava flow that drapes steeply over both the inner and outer walls of the caldera. Detailed petrographic and physical characteristics and the emplacement history of the flow can be found in Stevenson et al. (1993). The deposit is made up of finely vesicular pumice that forms a surface carapace and represents the upper 10 m of the flow. Below this follows a upper obsidian layer (UOBS) that gradually changes downwards to a central crystalline rhyolite layer. Beneath this rhyolite layer a lower obsidian layer (LOBS) that incorporates a basal crumble layer is found above the already mentioned fall deposit (Stevenson et al., 1993). Remnants of original ejecta and spatters within the lowermost part of LOBS give evidence that the flow was initially particulate as spatter from a lava fountain and deformed after emplacement (Stevenson et al., 1993).

All samples for this study were originally obtained by Gottsmann and Dingwell (2002) without orientation for their study on the thermal history of the 8 ka flow. A 70 cm thick vertical profile of LOBS (Fig. 3) was sampled at Hall's Pass which is an area where the flow drapes back into the caldera. Sample names indicate sample number and vertical position measured from top, i.e. LOBS2.13: sample 2, at depth of 13 cm. The sequence was taken above a crumble breccia containing disintegrated, slightly fused pumices from the underlying pumice deposit and clasts of the overlying obsidian. Towards the central crystalline rhyolite on top of LOBS a decimetre thick transition zone with obsidian fragments is incorporated into the rhyolite or in layers of folded glass and rock bands. In this transition zone gas blisters of ~10 cm are found. At Parikoura Point on the east coast of the island a horizontal profile was sampled through exposures of UOBS (Fig. 4). It consists of steeply inland dipping flow ridges and ramps. It was sampled at the northern cliff face along a slightly north-easterly inclined platform. The profile is ~30 m long and comprises a sequence of anticlinal flow ridges and synclinal troughs between these ridges. Samples were taken from the exposed surfaces of the flow ridges. Sample names give horizontal profile distance in cm, i.e. sample

---

## Paleointensity on 8 ka New Zealand obsidian

A. Ferk et al.

---

[Title Page](#)[Abstract](#)[Introduction](#)[Conclusions](#)[References](#)[Tables](#)[Figures](#)[Back](#)[Close](#)[Full Screen / Esc](#)[Printer-friendly Version](#)[Interactive Discussion](#)

UOBS1420 is at 14.20 m in the profile. One flow ridge was sampled in a 5.2 m long detailed profile with spacing of 20 to 50 cm (samples UOBS700 to UOBS1220). In the transition zone from the central crystalline rhyolite to the UOBS alternating bands of crystalline rhyolite and obsidian as well as an increase in bubble content are found. At the upper end of UOBS gas blisters and increasing vesicularity show the transition to the finely vesicular pumice layer (Stevenson et al., 1993).

Samples of both LOBS and UOBS are very pristine with no indication of secondary hydration or alteration processes. Both layers show very similar chemical composition with in average  $[\text{mol}(\text{Na}_2\text{O} + \text{K}_2\text{O})]/\text{Al}_2\text{O}_3$  of 1.54 (Gottsmann and Dingwell, 2002), which does not change with layer depth or horizontal sample location within the sites (Gottsmann and Dingwell, 2002).

### 3 Relaxation geospeedometry

Relaxation geospeedometry, i.e. measurements of the heat capacity at constant pressure  $c_p$ , can be used to determine both the glass transition temperature  $T_g$  and the natural cooling rate. The theoretical and mathematical background for this method has been discussed in detail by e.g. Wilding et al. (1995) and Gottsmann and Dingwell (2001). Here we only concentrate on the most important points. By passing through the glass transition, the melt changes from liquid-like viscous to solid-like brittle behavior (Dingwell and Webb, 1990); it goes from a thermodynamic state of metastable equilibrium to one of disequilibrium. Thus,  $T_g$  depends not only on the composition of the melt, but also on the quench rate. This information becomes frozen into the glass structure and can be gained by measurement of a structure-dependent physical property such as heat capacity  $c_p$ , during reheating. Formation of glass involves the freezing in of a structural arrangement that can be simplified by the concept of a fictive temperature  $T_f$  (Tool, 1946).  $T_f$  expresses the temperature at which the glass would be in equilibrium. Above the glass transition the relaxation time  $\tau$  to get back to equilibrium is short as the melt is in equilibrium and  $T_f$  equals the actual temperature  $T$ . At lower temperatures,

SED

3, 679–711, 2011

## Paleointensity on 8 ka New Zealand obsidian

A. Ferk et al.

Title Page

Abstract

Introduction

Conclusions

References

Tables

Figures

◀

▶

◀

▶

Back

Close

Full Screen / Esc

Printer-friendly Version

Interactive Discussion



more time is needed to reach equilibrium, i.e.  $\tau$  is larger, and the melt departs from equilibrium ( $T_f > T$ ). At this point the glass transition starts and it persists through a certain temperature interval. Below this interval the glass structure is frozen in and  $T_f$  is constant. Gottsmann and Dingwell (2002) use the limiting  $T_f$  to represent  $T_g$ , i.e. the lowest possible expression of  $T_g$  when the glass structure is completely frozen. Following the approach taken by Wilding et al. (1995) the Tool-Narayanaswamy-Moynihan equation (Narayanaswamy, 1971, 1988; DeBolt et al., 1976; Moynihan et al., 1976) for relaxation and for fictive temperature was used for this modelling.

Relaxation geospeedometry on LOBS and UOBS samples had already been performed by Gottsmann and Dingwell (2002). The data of these experiments is needed for cooling-rate correction of paleointensity experiments. Hence, a short summary of the experiment and their data are given: specimens for relaxation geospeedometry were prepared by drilling cylinders of 6 mm diameter from hand samples. These were then cleaned, dried for 24 h and stored in a desiccator until use. Two different differential scanning calorimeters (DSC) were used: a Setaram DSC 111 at the Bayerisches Geoinstitut, University of Bayreuth, Germany and a Netzsch DSC 404 at the University of Munich, Germany (indicated by superscript <sup>N</sup> in Table 1). For the Setaram DSC 10 mm long cores were placed in Pt capsules with both ends closed by Pt lids. For the Netzsch DSC 404 2–3 mm thick obsidian discs were hosted in Pt/Rh capsules. Calibration in both cases was against  $c_p$  of a single sapphire. After the first heating of the sample above  $T_g$ , it was cooled and heated in the DSCs with successive rates of 20, 16, 10, 8 and 5 K min<sup>-1</sup>. The five later runs which are no longer influenced by natural cooling allow an estimation of the sample specific parameters. These can then be used to fit the first run, by adapting the previous, i.e. natural, cooling rate.  $\pm 0.2 \log_{10}$  unit is a conservative estimate of the uncertainty in modelled cooling rates on the basis of repetitive sample analyses and of mismatch between  $c_p$  curves of samples and modelled cooling rate differences of one order of magnitude.

Modelled cooling rates range from 0.00072 K min<sup>-1</sup> to 6.3 K min<sup>-1</sup> (Table 1).  $T_g$  ranges between 489 °C and 405 °C. Within the vertical profile of LOBS cooling rates

SED

3, 679–711, 2011

**Paleointensity on 8 ka  
New Zealand  
obsidian**

A. Ferk et al.

Title Page

Abstract

Introduction

Conclusions

References

Tables

Figures

◀

▶

◀

▶

Back

Close

Full Screen / Esc

Printer-friendly Version

Interactive Discussion



increase from  $0.00072 \text{ K min}^{-1}$  close to the crystalline rhyolite to  $0.017 \text{ K min}^{-1}$  at the contact to the basal crumble breccia (Fig. 5). The centre of LOBS shows uniform cooling rates of  $\sim 0.001 \text{ K min}^{-1}$ . Most of the samples of UOBS show cooling rates between  $0.00102 \text{ K min}^{-1}$  (UOBS1080, Fig. 6) and  $0.01242 \text{ K min}^{-1}$  (UOBS2650) (Fig. 6). UOBS120 and UOBS2095 show a much faster cooling rates of  $6.3 \text{ K min}^{-1}$  and  $2.5 \text{ K min}^{-1}$ , respectively.

#### 4 Magnetic mineralogy and domain state

Rock magnetic measurements were performed to analyze magnetic mineralogy and domain state. Isothermal remanent magnetization (IRM) acquisition, isothermal backfield curves, hysteresis loops (all at room temperature) and thermomagnetic curves were measured on a Variable Field Translation Balance (VFTB) by Petersen Instruments at the University of Munich, Germany using 8 mm diameter miniature cores. Further, hysteresis and backfield curves (at low, room and high temperatures) were done on a low-temperature (LT) Vibrating Sample Magnetometer (VSM) and on a high-temperature (HT) VSM (both by Princeton Measurements). For some samples also the dependences of hysteresis and backfield on temperature were measured on LTVSM and/or HTVSM. Additionally, thermomagnetic curves were measured with the HTVSM. Last but not least, different low temperature experiments were done on a Magnetic Properties Measurement System (MPMS) by Quantum Design. LTVSM, HTVSM and MPMS experiments were done in the course of a visitor's fellowship at the Institute for Rock Magnetism at the University of Minneapolis, USA.

Three LOBS (1.4, 4.33, 8.73) and five UOBS (120, 295, 925, 1420, 2095) samples were measured in the VFTB and the according data was analyzed using the RockMagAnalyzer software by Leonhardt (2006). All three LOBS samples are mainly paramagnetic, but have a remanent content that is high enough to get good IRM and backfield curves (Fig. 7a i). For samples LOBS1.4 and 8.73 it is also possible to determine a Curie temperature  $T_C$  of  $\sim 210^\circ\text{C}$  (Fig. 7a iii) even though the departure of the

SED

3, 679–711, 2011

### Paleointensity on 8 ka New Zealand obsidian

A. Ferik et al.

Title Page

Abstract

Introduction

Conclusions

References

Tables

Figures

◀

▶

◀

▶

Back

Close

Full Screen / Esc

Printer-friendly Version

Interactive Discussion



---

**Paleointensity on 8 ka  
New Zealand  
obsidian**A. Ferk et al.

---

Title Page

Abstract

Introduction

Conclusions

References

Tables

Figures

◀

▶

◀

▶

Back

Close

Full Screen / Esc

Printer-friendly Version

Interactive Discussion



thermomagnetic curves from a curve calculated for the decrease in saturation magnetisation of paramagnetic particles (green line in Fig. 7a iii) is not very strong. For  $T_C$  determination this paramagnetic decrease was subtracted from the original thermomagnetic curve. Later remanence measurements (Sect. 5) shows unblocking of grains in LOBS8.73 up to at least 400 °C. This implies a contribution from remanence carriers that do not show in the thermomagnetic curves due to the high paramagnetic contribution. Plotting of  $M_{rs}/M_s$  and  $B_{cr}/B_c$  for these two samples (LOBS1.4 and 8.73) in a Day plot shows their single domain (SD) characteristics. The hysteresis loop of sample LOBS4.33 is very thin and thus, no meaningful hysteresis parameters can be obtained. Samples from UOBS are even more paramagnetic than LOBS4.33. Hysteresis measurements show only a slightly broadened straight line through the origin (Fig. 7b ii) and IRM and backfield measurements are very noisy even though a remanent contribution can clearly be seen (Fig. 7b i). For thermomagnetic curves deviations from the paramagnetic decrease are so small that no Curie temperatures can be determined (Fig. 7b iii).

As the very strong paramagnetic contribution mostly prevented obtaining meaningful data using the VFTB, further measurements were done on the more sensitive MPMS and VSMs. However, their higher sensitivity could not totally make up for the smaller sample sizes and so again mainly the strong paramagnetic contribution was monitored: Hysteresis and backfield data at room temperature (RT) were taken for every sample. Hysteresis plots are almost always dominated by the paramagnetic contribution (e.g. UOBS 1080 in Fig. 8a i). A small ferrimagnetic contribution can be seen when the loops are corrected for the high field slope (Fig. 8a ii), but the measurement noise is much too high to determine hysteresis parameters. Only sample UOBS1945 (Fig. 8b i) shows a stronger hysteresis, but again the corrected loop is too thin to determine  $H_C$  (Fig. 8b ii). Further, it was impossible to determine  $H_{Cr}$  values from the backfield curves as there is always some shift in the data: Fig. 8a iii shows that at the end of the measurement not the same absolute value in magnetization as before was obtained. For some samples the y-axis was not even crossed. It was not possible to find any reason for this

shift and hence, no correction could be applied. For samples LOBS4.33, UOBS295 and UOBS1945 hysteresis and for UOBS1080 hysteresis and backfield curves were also measured in 10 °C steps from 10 K to room temperature and in 25 °C steps from room temperature to ~450 °C. However, no further insights regarding the remanence carriers could be gained from these measurements as the paramagnetic contribution stayed dominant during the hysteresis loops and backfield measurements were as erroneous as those at room temperature. Thermomagnetic curves for LOBS7.63 and UOBS700 are also similar to those of the VFTB. They only show slight deviations from paramagnetic decay. For UOBS700 a little kink below ~400 °C implies a Curie temperature in this range, but the data is not very clear. For low temperature experiments in the MPMS fields at room temperature (RT), at low temperature (LT, 10 K) or during cooling of 2.5 T were applied and the field was turned off during the measurement: A RTSIRM (room temperature SIRM) was implied on samples LOBS4.33, UOBS295 and UOBS1945 and measured during cooling to 10 K, then a LTSIRM (low temperature SIRM) was implied and measured during warming to RT (Fig. 9a, b and c). Sample UOBS1080 experienced a more detailed measurement procedure: After field-cooling (FC) to 10 K, this FC remanence was measured during warming to RT. After another cooling to 10 K a LTSIRM was applied and measured during warming to RT. Then a RTSIRM was applied and measured during cooling to 10 K and during warming to RT (Fig. 9d). Neither at ~262 K (Hematite Morin transition) nor at ~120 K (Magnetite Verwey Transition) are any remarkable changes in the different remanent magnetizations observed. However, there is always a strong decrease in RTSIRM during cooling and a respective increase in LTSIRM below 50–75 K. This is most probably connected to the high paramagnetic/ferro(i)magnetic ratio: Within the MPMS the field is not perfectly zeroed. There seems to be a small negative residual field of  $\pm 1\text{--}2\ \mu\text{T}$ . Paramagnetic susceptibility is inversely proportional to temperature and, thus, at low temperatures an induced negative magnetization partially cancels out the positive remanence. Sample UOBS295 (Fig. 9b) shows a more sharp decrease in RTSIRM during cooling which hints to ordering or a phase transition rather than to gradual increase in paramagnetic

---

**Paleointensity on 8 ka  
New Zealand  
obsidian**A. Ferk et al.

---

[Title Page](#)[Abstract](#)[Introduction](#)[Conclusions](#)[References](#)[Tables](#)[Figures](#)[⏪](#)[⏩](#)[◀](#)[▶](#)[Back](#)[Close](#)[Full Screen / Esc](#)[Printer-friendly Version](#)[Interactive Discussion](#)

susceptibility. However, the LTSIRM warming curve does not show a sudden increase and an interpretation is therefore difficult. All warming curves show decreases above 50–75 K. Such decreases may have different reasons like unblocking of superparamagnetic (SP) grains or domain reorganization in MD high-Ti titanomagnetite (Moskowitz et al., 1998). However, for our samples VFTB experiments have shown that we are dealing with SD or close to SD remanence carriers. Hence, the second possibility can be ruled out and instead it is followed that nanoparticles go from SP to stable SD. The difference between FC remanence and LTSIRM warming curves in Fig. 9d suggests the presence of a hard phase (e.g. an imperfect antiferromagnet) with a low ordering temperature (50–100 K) that is magnetized more efficiently by field-cooling (strong-field TRM) than isothermally at 10 K.

An identification of remanence carriers is not possible based on the so far performed VFTB, VSM and MPMS experiments. The strong paramagnetic contribution constrains analysis of the ferro(i)magnetic particles. However, the small grain sizes and the small but clearly existing remanence suggest that paleointensity determination is worth a try.

## 5 Paleointensity determination

### 5.1 Thellier-type experiments

Paleointensity experiments on 8 mm diameter miniature cores and on inch cores were done in a MMTD20 thermal demagnetizer in the paleomagnetic laboratory of the University of Munich, Germany in Niederlippach and in a MMTD60 thermal demagnetizer in the laboratory of the Montan University Leoben, Austria in Gams. For in-field steps laboratory fields of  $30 \pm 0.1 \mu\text{T}$  were applied during heating and cooling. The experiments followed the modified Thellier-technique MT4 by Leonhardt et al. (2004a) which is a zero-field first method that incorporates pTRM checks, additivity checks (Krása et al., 2003) and pTRM tail checks (Riisager and Riisager, 2001). Directional differences between the applied field and the NRM of the pTRM-tail check are taken into

SED

3, 679–711, 2011

## Paleointensity on 8 ka New Zealand obsidian

A. Ferk et al.

Title Page

Abstract

Introduction

Conclusions

References

Tables

Figures

◀

▶

◀

▶

Back

Close

Full Screen / Esc

Printer-friendly Version

Interactive Discussion



account according to Leonhardt et al. (2004b). All determinations were analyzed using the ThellierTool4.21 software and its default criteria (Leonhardt et al., 2004a). Paleointensity data are summarized in Table 2 with sample subscripts m, NL and G denoting minicores, Niederlippach and Gams, respectively, and different Arai plots are given in Fig. 10.

Measurements in Niederlippach were proceeded to temperatures above  $T_g$  even though  $NRM_{left}$  had already been only  $\sim 10\%$  at  $\sim 390^\circ\text{C}$ . Alteration of these samples gets very strong above  $T_g$  leading to departing checks (e.g. Fig. 10a). As this alteration is most likely connected to relaxation of the glass structure, only steps below  $T_g$  are considered for paleointensity determination, i.e. only steps up to  $390^\circ\text{C}$  (7 steps), while higher temperature steps are disregarded. This accounts for the two miniature samples LOBS8.73 and UOBS2095 as well as for the 8 inch cores measured in Niederlippach (subscript NL in Table 2). With this experience in mind, 24 samples (inch cores) in the Gams laboratory were heated up to  $390^\circ\text{C}$  in 10 steps. Almost all samples were then demagnetized to at least 15%. Only samples UOBS889 (Fig. 10d), 1570 and 2380 had  $\sim 20\%$ , UOBS0  $\sim 40\%$  and UOBS1945 and 2095  $\sim 50\%$  left.

Paleointensity determinations are of good quality. In total data from 24 of the 34 measured samples (70%) could be used with good values for different quality parameters: Mostly fraction of the NRM  $f$  (Coe et al., 1978) and gap factor  $g$  (Coe et al., 1978) are greater than 0.7, quality factor  $q$  (Coe et al., 1978) ranges between 8 and 100, though mostly between 15 and 20. In many of the experiments an onset of alteration is observed at higher temperature steps above  $\sim 300^\circ\text{C}$  which is probably related to the repeated heating to temperatures close to  $T_g$ . However, for the temperature intervals used for paleointensity determination mostly  $DRAT \leq 5.1$  (Selkin and Tauxe, 2000) and hence the data should be reliable. Repeated thermal demagnetizations show only minor deviations ( $d(TR) \leq 2.1\%$ ) indicative of SD remanence carriers for 63% of the samples and slightly higher values (up to  $d(TR) = 5.5\%$ ) indicative of small PSD particles for the others although an unique interpretation in terms of domain size is hampered by the above mentioned alterations above  $\sim 300^\circ\text{C}$  before the remanence is unblocked.

## Paleointensity on 8 ka New Zealand obsidian

A. Ferk et al.

[Title Page](#)[Abstract](#)[Introduction](#)[Conclusions](#)[References](#)[Tables](#)[Figures](#)[◀](#)[▶](#)[◀](#)[▶](#)[Back](#)[Close](#)[Full Screen / Esc](#)[Printer-friendly Version](#)[Interactive Discussion](#)

Arithmetic means and standard deviations for LOBS and UOBS are  $56.5 \pm 2.0 \mu\text{T}$  and  $59.2 \pm 8.4 \mu\text{T}$ , respectively. For the whole 8 ka flow a weighted mean (using  $1/(\text{arithmetic standard deviation})$  as weighting factor) of  $57.0 \pm 1.0 \mu\text{T}$  is calculated.

## 5.2 Anisotropy correction

As samples in Niederlippach had been heated too high, no anisotropy or cooling rate experiments (Sect. 5.3) could be performed on these samples. Relaxation at the glass transition altered the samples and no meaningful results can be obtained.

However, for Gams samples these experiments could be carried out. If a rock is magnetic anisotropic this means that its ability to acquire a magnetization in a magnetic field depends on its orientation with respect to that field. The anisotropy tensor of TRM (ATRM tensor) can be obtained as weak field TRM is proportional to the field strength. Determinations of the ATRM tensor were done on the same samples as paleointensity determinations in the MMTD60 demagnetizer in the Gams laboratory. TRMs were imparted using in-field heating/cooling cycles to the upper end of the blocking spectra of the samples, i.e. up to  $390^\circ\text{C}$ , subsequently in +z, +x, -x, +y, -y and -z direction. Additionally, the +z treatment was repeated in the end to check for alteration. The measurements were analyzed following the approach of Veitch et al. (1984) and the results are summarized in Table 2: After determining the ATRM tensor, the direction of the ancient field is calculated and the scaling factor  $f_{\text{ATRM}}$  to adjust the measured paleointensity by  $H_{\text{ATRM}} = H_{\text{UC}} \cdot f_{\text{ATRM}}$  (UC: uncorrected), is finally obtained by the relationship between ancient magnetization acquisition and laboratory magnetization acquisition in dependence of the ATRM tensor.  $f_{\text{ATRM}}$  is not only determined from the averaged axes components but also separately for positive (+x, +y, +z) and negative (-x, -y, -z) measurements, i.e.  $f_{\text{ATRM}}^{\text{pos}}$  and  $f_{\text{ATRM}}^{\text{neg}}$ . The uncertainty of  $f_{\text{ATRM}}$  is calculated by  $\sigma(f_{\text{ATRM}}) = (|f_{\text{ATRM}}^{\text{pos}} - f_{\text{ATRM}}^{\text{neg}}|)$ . The uncertainty  $\sigma(H_{\text{ATRM}})$  of the ATRM corrected paleointensity is a minimum-maximum error including the uncertainty of the uncorrected paleointensity  $\sigma(H)$  and of the correction factor  $\sigma(f_{\text{ATRM}})$ .

## Paleointensity on 8 ka New Zealand obsidian

A. Ferk et al.

Title Page

Abstract

Introduction

Conclusions

References

Tables

Figures

◀

▶

◀

▶

Back

Close

Full Screen / Esc

Printer-friendly Version

Interactive Discussion



For only 8 of the 24 samples was alteration small enough to correct for anisotropy. Figure 11 shows that in most cases the two +z measurements at the beginning and at the end of the experiment varied by  $\geq 5\%$ . Therefore, anisotropy correction was tried only for samples LOBS5.42, UOBS720, 775, 889, 1570, 1705, 1945 and 2095.

As mentioned above samples UOBS889, 1570, 1945 and 2095 still have  $NRM_{\text{left}} > 15\%$  at  $390^\circ\text{C}$ . As their  $T_g$  is in the same range as the one of the other samples, it was decided to stop heating them further and to determine also for them the ATRM tensor at  $390^\circ\text{C}$ . By vector subtraction of the remaining TRM as measured after the last paleointensity step from every step during the anisotropy experiment a reasonable measure of the tensor should be yielded. Although TRM capacity remained stable as has been shown by the  $\leq 5\%$  difference between the two +z measurements, very high relative errors  $\sigma(f_{\text{ATRM}})/f_{\text{ATRM}}$  of 11–164% were found for most samples (data for  $f_{\text{ATRM}}$  and  $H_{\text{ATRM}}$  in brackets in Table 2). These high errors suggest that there was alteration during these experiments that was not monitored by the two +z measurements. Either alteration did not affect the tensor in this direction or it was just by chance that these two measurements showed similar values. Only samples UOBS889, 1570 and 2095 showed relative errors  $< 5\%$  that were thought to represent reliable measurements. Thus, for the anisotropy corrected paleointensity values of  $61.1 \pm 8.9 \mu\text{T}$  for UOBS and  $59.3 \pm 2.2 \mu\text{T}$  for the whole flow only corrected paleointensities of these three samples and uncorrected paleointensities of all other samples were used. In both cases the paleointensity is slightly increased but with-in error identical to the uncorrected mean values.

### 5.3 Corrections for cooling rate dependence

In the 1980s several studies (Halgedahl et al., 1980; Dodson and McClelland-Brown, 1980; Fox and Aitken, 1980; McClelland-Brown, 1984) have shown that non-interacting SD particles acquire a smaller TRM during faster cooling. How exactly the TRM depends on cooling rate varies, however, already with slight changes in grain size and domain state. Hence, to correct overestimation of paleointensity (Leonhardt et al., 2006;

SED

3, 679–711, 2011

## Paleointensity on 8 ka New Zealand obsidian

A. Ferk et al.

Title Page

Abstract

Introduction

Conclusions

References

Tables

Figures

◀

▶

◀

▶

Back

Close

Full Screen / Esc

Printer-friendly Version

Interactive Discussion







out data that was obtained above  $T_g$  and it was not possible to perform ATRM or CR correction on all samples. Nevertheless, the successful ATRM and CR experiments indicate negligible difference to uncorrected data. The uncorrected mean paleointensity of  $57.0 \pm 1.0 \mu\text{T}$  seems most reliable and can at least give a upper limit of the field strength 8 ka ago in New Zealand as faster cooling in the laboratory compared to nature leads to an overestimate of paleointensity when dealing with SD remanence carriers (Halgedahl et al., 1980; Dodson and McClelland-Brown, 1980). Interestingly, a comparison with previous intensity data from the same region shows excellent agreement: Within error our Mayor Island paleointensity data for  $6050 \pm 70$  BCE is identical to the field value of  $58.1 \pm 2.9 \mu\text{T}$  which Tanaka et al. (2009) obtained for a  $\sim 500$  year younger (5500 BCE) rhyolitic lava at Okataina Volcanic Center (OVC). OVC is a rhyolitic eruptive center within Taupo Volcanic Zone and just  $\sim 100$  km distant from Mayor Island. Tanaka et al. (2009) did not apply any cooling-rate correction. Normally one would expect different cooling rate dependencies. The match in the uncorrected data may be fortuitous especially when considering the 500 year age difference. However, it might also indicate that in these cases the cooling rate does not have a strong influence. Further studies will have to check this. Tanaka et al. (2009) have also compared their data to other volcanic and lake sediment data and to the geomagnetic field model CALS7K by Korte and Constable (2005). While the paleointensity data itself agrees well with a world-wide trend with a moderate high at 7–8 ka (Yang et al., 2000), there is a very poor fit to CALS7K. This is reasonable considering the paucity of reliable paleointensity data in the Pacific region to date and the thereby induced strong weighting of sedimentary data in the model. Further, geomagnetic field models are always less free to develop close to boundary due to the necessary boundary conditions. This may introduce additional errors at locations with few data. A comparison of our data with CALS7K is not possible as the model does not go back far enough. Therefore, agreement of the data with the so far unpublished geomagnetic field model by Leonhardt et al. (2010) that goes back to 10 ka was tested. This model suggests a field value of  $\sim 43.5 \mu\text{T}$  for  $6050 \pm 70$  BCE at Mayor Island. Mainly this will again be due to the

---

## Paleointensity on 8 ka New Zealand obsidian

A. Ferk et al.

---

Title Page

Abstract

Introduction

Conclusions

References

Tables

Figures

◀

▶

◀

▶

Back

Close

Full Screen / Esc

Printer-friendly Version

Interactive Discussion



low number of data constraining the model at this time strengthening again the need for more and better data. Our new paleointensity value itself is of high quality. It is therefore, an important first step towards a better global distribution of high quality data and better-defined geomagnetic field models.

5 *Acknowledgements.* We are very thankful to J. Gottsmann for providing maps and figures of his study (Gottsmann and Dingwell, 2002). Rockmagnetic measurements at the Institute for Rock Magnetism were enabled by a Visiting Fellowship for A. Ferk. Our warmest thanks go to the whole IRM staff, especially to Mike Jackson, for their help with the equipment and with interpretation of low temperature data. Further thanks to Karl Fabian for help with mathematica.  
10 Funding was provided by DFG grant Le1905/1-1 and FWF grant P21221-N14. D. B. Dingwell acknowledges the funding support of a LMUexcellent Research Professorship in experimental Volcanology (Bundesexzellenzinitiative) and ERC advanced grant EVOKES.

## References

- 15 Bowles, J., Gee, J. S., Kent, D. V., Bergmanis, E., and Sinton, J.: Cooling rate effects on paleointensity estimates in submarine basaltic glass and implications for dating young flows, *Geochem. Geophys. Geosys.*, 6, Q07002, doi:10.1029/2004GC000900, 2005. 681
- Buck, M. D., Briggs, R. M., and Nelson, C. S.: Pyroclastic deposits and volcanic history of Mayor Island, N Z J. Geol. Geophys., 24, 449–4667, 1981. 682
- 20 Coe, R. S., Grommé, S., and Mankinen, E. A.: Geomagnetic paleointensities from radiocarbon-dated lava flows on Hawaii and the question of the Pacific nondipole low, *J. Geophys. Res.*, 83, 1740–1756, 1978. 689
- Cottrell, R. D. and Tarduno, J. A.: Geomagnetic paleointensity derived from single plagioclase crystals, *Earth Planet. Sci. Lett.*, 169, 1–5, 1999. 681
- 25 DeBolt, M. A., Easteal, A. J., Macedo, P. B., and Moynihan, C. T.: Analysis of structural relaxation in glass using rate heating data, *J. Am. Ceram. Soc.*, 59, 16–21, 1976. 684
- Dekkers, M. J. and Bönhel, H. N.: Reliable absolute palaeointensities independent of magnetic domain state, *Earth Planet. Sci. Lett.*, 248, 508–517, 2006. 681
- Dingwell, D. B. and Webb, S. L.: Relaxation in silicate melts, *Eur. J. Mineral.*, 2, 427–449, 1990. 683

## Paleointensity on 8 ka New Zealand obsidian

A. Ferk et al.

Title Page

Abstract

Introduction

Conclusions

References

Tables

Figures



Back

Close

Full Screen / Esc

Printer-friendly Version

Interactive Discussion



- Dodson, M. H. and McClelland-Brown, E.: Magnetic blocking temperatures of single-domain grains during slow cooling, *J. Geophys. Res.*, 85, 2625–2637, 1980. 691, 692, 694
- Fabian, K. and Leonhardt, R.: Multiple-specimen absolute paleointensity determination: An optimal protocol including pTRM normalization, domain-state correction, and alteration test, *Earth Planet. Sci. Lett.*, 297, 84–94, 2010. 681
- Ferk, A., v. Aulock, F. W., Leonhardt, R., Hess, K.-U., and Dingwell, D. B.: A cooling rate bias in paleointensity determination from volcanic glass: an experimental demonstration, *J. Geophys. Res.*, 115, B08102, 1–8, 2010. 692
- Fox, J. M. W. and Aitken, M. J.: Cooling-rate dependency of thermoremanent magnetisation, *Nature*, 283, 462–463, 1980. 691
- Gottsmann, J. and Dingwell, D. B.: The cooling of frontal flow ramps: a calorimetric study on the Rocche Rosse rhyolite flow, Lipari, Aeolian Islands, Italy, *Terra Nova*, 19, 157–164, 2001. 683
- Gottsmann, J. and Dingwell, D. B.: The thermal history of a spatter-fed lava flow: the 8-ka pantellerite flow of Mayor Island, New Zealand, *Bull. Volcanol.*, 64, 410–422, 2002. 682, 683, 684, 695, 702, 703, 704, 705, 706
- Halgedahl, S. L., Day, R., and Fuller, M.: The effect of cooling rate on the intensity of weak-field TRM in single-domain magnetite, *J. Geophys. Res.*, 85, 3690–3698, 1980. 691, 692, 694
- Houghton, B. F. and Wilson, C. J. N.: Explosive rhyolitic volcanism: the case studies of Mayor Island and Taupo Volcanoes, *N Z Geol. Surv. Records*, 12, 33–100, 1986. 681, 682
- Houghton, B. F., Weaver, S. D., Wilson, C. J. N., and Lanphere, M. A.: Evolution of a Quaternary peralkaline volcano; Mayor Island, New Zealand, *J. Vol. Geoth. Res.*, 51, 217–236, 1992. 681
- Korte, M. and Constable, C. G.: Continuous geomagnetic field models for the past 7 millennia: 2. CALS7K, *Geochem. Geophys. Geosys.*, 6, Q02H16, doi:10.1029/2004GC000801, 2005. 681, 694
- Krása, D., Heunemann, C., Leonhardt, R., and Petersen, N.: Experimental procedure to detect multidomain remanence during Thellier-Thellier experiments, *Phys. Chem. Earth*, 28, 681–687, 2003. 688
- Leonhardt, R.: Analyzing rock magnetic measurements: The RockMagAnalyzer 1.0 software, *Computers & Geosciences*, 32, 1420–1431, 2006. 685
- Leonhardt, R., Fabian, K., and Schnepf, E.: Holocene global geomagnetic field reconstruction based on archeomagnetic data: Assessing error sources and uncertainties, *EGU General Assembly*, Vienna, Austria, 2–7 May 2010, EGU2010–9421, 2010. 694

---

**Paleointensity on 8 ka  
New Zealand  
obsidian**A. Ferk et al.

---

[Title Page](#)[Abstract](#)[Introduction](#)[Conclusions](#)[References](#)[Tables](#)[Figures](#)[Back](#)[Close](#)[Full Screen / Esc](#)[Printer-friendly Version](#)[Interactive Discussion](#)

---

**Paleointensity on 8 ka  
New Zealand  
obsidian**A. Ferk et al.

---

[Title Page](#)[Abstract](#)[Introduction](#)[Conclusions](#)[References](#)[Tables](#)[Figures](#)[◀](#)[▶](#)[◀](#)[▶](#)[Back](#)[Close](#)[Full Screen / Esc](#)[Printer-friendly Version](#)[Interactive Discussion](#)

- Leonhardt, R., Heunemann, C., and Krása, D.: Analyzing absolute paleointensity determinations: Acceptance criteria and the software ThellierTool4.0, *Geochem. Geophys. Geosys.*, 5, Q12016, doi:10.1029/2004GC000807, 2004a. 688, 689
- Leonhardt, R., Krása, D., and Coe, R. S.: Multidomain behavior during Thellier paleointensity experiments: A phenomenological model, *Phys. Earth Planet. Inter.*, 147, 127–140, 2004b. 680, 689
- Leonhardt, R., Matzka, J., Nichols, A. R. L., and Dingwell, D. B.: Cooling rate correction of paleointensity determination for volcanic glasses by relaxation geospeedometry, *Earth Planet. Sci. Lett.*, 243, 282–292, 2006. 680, 681, 691, 692
- Macdonald's, R. A.: Nomenclature and petrochemistry of the peralkaline oversaturated extrusive rocks, *Bull. Volcanol.*, 38, 498–516, 1974. 681
- McClelland-Brown, E.: Experiments on TRM intensity dependence on cooling rate, *Geophys. Res. Lett.*, 11, 205–208, 1984. 691
- Moskowitz, B. M., Jackson, M., and Kissel, C.: Low-temperature magnetic behavior of titanomagnetites, *Earth Planet. Sci. Lett.*, 157, 141–149, 1998. 688
- Moynihan, C. T., Eastal, A. H., DeBolt, M. A., and Tucker, J.: Dependence of fictive temperature of glass on cooling rate, *J. Am. Ceram. Soc.*, 59, 12–16, 1976. 684
- Muxworthy, A. R. and Heslop, D.: A Preisach method for estimating absolute paleofield intensity under the constraint of using only isothermal measurements: 1. Theoretical framework, *J. Geophys. Res.*, 116, B04102, doi:10.1029/2010JB007843, 2011. 681
- Narayanaswamy, O. S.: A model of structural relaxation in glass, *J. Am. Ceram. Soc.*, 54, 491–498, 1971. 684
- Narayanaswamy, O. S.: Thermorheological simplicity in the glass transition, *J. Am. Ceram. Soc.*, 71, 900–904, 1988. 684
- Pick, T. and Tauxe, L.: Geomagnetic paleointensities: Thellier experiments on submarine basaltic glass from the East Pacific Rise, *J. Geophys. Res.*, 98, 17949–17964, 1993. 681
- Riisager, P. and Riisager, J.: Detecting multidomain magnetic grains in Thellier paleointensity experiments, *Phys. Earth Planet. Inter.*, 125, 111–117, 2001. 688
- Selkin, P. A. and Tauxe, L.: Long-term variations in paleointensity, *Phil. Trans. R. Soc.*, 358, 1065–1088, 2000. 689
- Smirnov, A. V. and Tarduno, J. A.: Magnetic hysteresis monitoring of Cretaceous submarine basaltic glass during Thellier paleointensity experiments: evidence for alteration and attendant low field bias, *Earth Planet. Sci. Lett.*, 206, 571–585, 2003. 693

---

## Paleointensity on 8 ka New Zealand obsidian

A. Ferk et al.

---

Title Page

Abstract

Introduction

Conclusions

References

Tables

Figures

◀

▶

◀

▶

Back

Close

Full Screen / Esc

Printer-friendly Version

Interactive Discussion



- Stevenson, R. J., Briggs, R. M., and Hodder, A. P. W.: Emplacement history of a low viscosity, fountain-fed pantelleritic lava flow, *J. Vol. Geoth. Res.*, 57, 39–56, 1993. 681, 682, 683
- Tanaka, H., Komuro, N., and Turner, G. M.: Palaeosecular variation for 0.1–21 Ka from the Okataina Volcanic Centre, New Zealand, *Earth Planets Space*, 61, 213–225, 2009. 680, 694
- 5 Tarduno, J. A., Cottrell, R. D., Watkeys, M. K., and Bauch, D.: Geomagnetic field strength 3.2 billion years ago recorded by single silicate crystals, *Nature*, 446, 657–660, 2007. 681
- Tool, A. Q.: Relation between inelastic deformability and thermal expansion of glass in its annealing range, *J. Am. Ceram. Soc.*, 29, 240–253, 1946. 683
- 10 Valet, J.-P., Brassart, J., Le Meur, I., Soler, V., Quidelleur, X., Tric, E., and Gillot, P.-Y.: Absolute paleointensity and magnetomineralogical changes, *J. Geophys. Res.*, 101(B11), 25029–25044, 1996. 680
- Veitch, R. J., Hedley, I. G., and Wagner, J.-J.: An investigation of the intensity of the geomagnetic field during Roman times using magnetically anisotropic bricks and tiles, *Arch. Sc. Genève*, 37, 359–373, 1984. 680, 690
- 15 Wilding, M. C., Webb, S. L., and Dingwell, D. B.: Evaluation of a relaxation geospeedometer for volcanic glasses, *Chem. Geol.*, 125, 137–148, 1995. 683, 684
- Yang, S., Odah, H., and Shaw, J.: Variations in the geomagnetic dipole moment over the last 12000 years, *Geophys. J. Int.*, 140, 158–162, 2000. 694

**Table 1.** Relaxation geospeedometry.

Sample	Limiting $T_f$ [°C]	natural cooling rate [K min <sup>-1</sup> ]
LOBS1.4	407	0.00072
LOBS2.13	409	0.00084
LOBS3.23	409	0.00114
LOBS4.33	412	0.0012
LOBS5.42	411	0.00114
LOBS6.53	420	0.0012
LOBS7.63	425	0.00174
LOBS8.73	454	0.01692
UOBS0	429	0.00378
UOBS120 <sup>N</sup>	489	6.3
UOBS225 <sup>N</sup>	444	0.009
UOBS295	449	0.01122
UOBS700	411	0.0015
UOBS720 <sup>N</sup>	425	0.0051
UOBS750 <sup>N</sup>	454	0.00672
UOBS775 <sup>N</sup>	450	0.00726
UOBS837 <sup>N</sup>	447	0.00606
UOBS889 <sup>N</sup>	452	0.00588
UOBS925 <sup>N</sup>	412	0.00282
UOBS986 <sup>N</sup>	420	0.00144
UOBS1020 <sup>N</sup>	415	0.0012
UOBS1080 <sup>N</sup>	405	0.00102
UOBS1117 <sup>N</sup>	420	0.0012
UOBS1153 <sup>N</sup>	413	0.00114
UOBS1220	453	0.0057
UOBS1420	417	0.00192
UOBS1570	411	0.00174
UOBS1705 <sup>N</sup>	432	0.0063
UOBS1825	418	0.00336
UOBS1945	444	0.0087
UOBS2095 <sup>N</sup>	486	2.52
UOBS2245	419	0.00222
UOBS2380	430	0.00516
UOBS2650	448	0.01242

Limiting fictive temperatures  $T_f$  and natural cooling rates of indicated samples. The limiting fictive temperature  $T_f$  is used to represent  $T_g$ . It constitutes the temperature of the undercooled melt at which the glass structure is completely frozen in without any possibility for further structural relaxation, i.e. the lowest possible expression of  $T_g$ .

## Paleointensity on 8 ka New Zealand obsidian

A. Ferk et al.

Title Page

Abstract

Introduction

Conclusions

References

Tables

Figures

◀

▶

◀

▶

Back

Close

Full Screen / Esc

Printer-friendly Version

Interactive Discussion



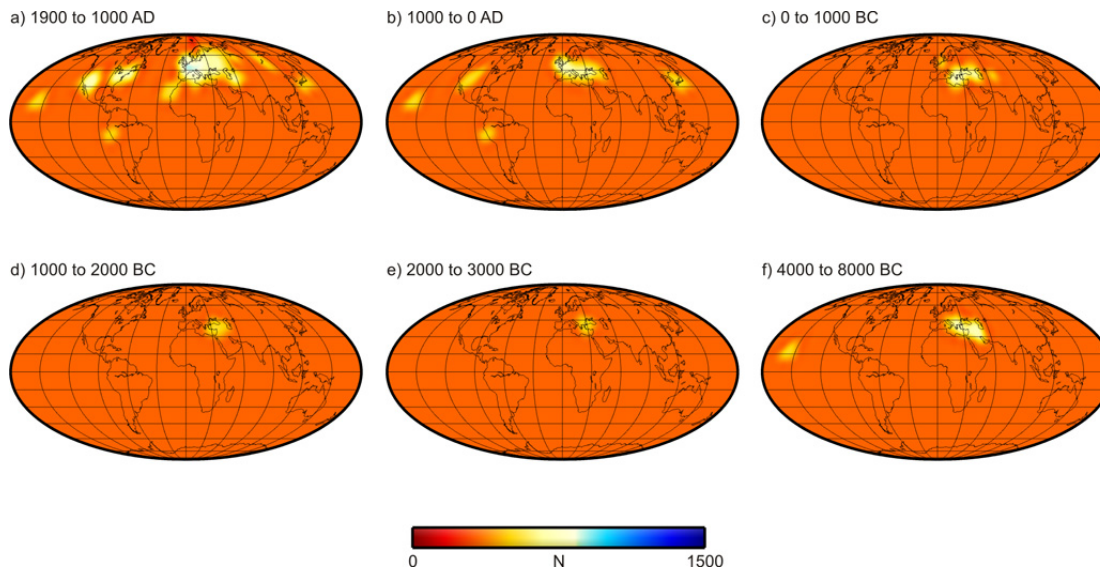
**Table 2.** Paleointensity results and correction.

Sample	Uncorr. paleointensity	ATRM correction		CR correction	
	$H_{UC}$ [ $\mu$ T]	$f_{ATRM}$	$H_{ATRM}$ [ $\mu$ T]	$f_{CR}$	$H_{ATRM,CR}$ [ $\mu$ T]
LOBS	56.5 ± 2.0				
LOBS2.13 <sub>NL</sub>	57.1 ± 1.9				
LOBS3.23 <sub>G</sub>					
LOBS4.33 <sub>NL</sub>	55.5 ± 1.2				
LOBS5.42 <sub>G</sub>	58.3 ± 1.1	(1.244 ± 0.218)	(72.5 ± 14.1)		
LOBS6.53 <sub>G</sub>					
LOBS6.53 <sub>NL</sub>	58.9 ± 4.2				
LOBS7.63 <sub>G</sub>	53.5 ± 0.9				
LOBS8.73 <sub>m</sub>					
LOBS8.73 <sub>NL</sub>	56.0 ± 1.9				
UOBS	59.2 ± 8.4				
UOBS0 <sub>G</sub>					
UOBS120 <sub>G</sub>	65.2 ± 2.0				
UOBS225 <sub>G</sub>	68.7 ± 2.9				
UOBS295 <sub>G</sub>	73.9 ± 2.9				
UOBS700 <sub>G</sub>	42.3 ± 0.4				
UOBS700 <sub>NL</sub>	59.0 ± 2.1				
UOBS701 <sub>G</sub>					
UOBS720 <sub>G</sub>	46.9 ± 2.5	(1.190 ± 1.950)	(55.8 ± 94.4)		
UOBS750 <sub>G</sub>	72.5 ± 3.2				
UOBS775 <sub>G</sub>	56.6 ± 0.4	(1.051 ± 0.278)	(59.5 ± 16.2)		
UOBS837 <sub>NL</sub>					
UOBS889 <sub>G</sub>	63.7 ± 1.4	1.113 ± 0.037	70.9 ± 3.9	1.106 ± 0.074	64.1 ± 0.7
UOBS925 <sub>NL</sub>	54.6 ± 2.4				
UOBS1020 <sub>G</sub>	58.0 ± 2.7				
UOBS1080 <sub>NL</sub>	64.1 ± 2.3				
UOBS1117 <sub>G</sub>					
UOBS1420 <sub>G</sub>					
UOBS1570 <sub>G</sub>	56.3 ± 1.4	1.238 ± 0.013	69.7 ± 2.4		
UOBS1705 <sub>G</sub>	53.1 ± 1.7	(1.067 ± 0.119)	(56.6 ± 8.1)		
UOBS1825 <sub>G</sub>					
UOBS1945 <sub>G</sub>	62.7 ± 2.0	(0.929 ± 0.239)	(58.2 ± 16.8)		
UOBS2095 <sub>m</sub>					
UOBS2095 <sub>G</sub>	50.1 ± 1.9	1.159 ± 0.050	58.0 ± 4.7		
UOBS2245 <sub>G</sub>	62.3 ± 2.6				
UOBS2380 <sub>G</sub>	55.2 ± 1.9				
8 ka flow	57.0 ± 1.0		59.3 ± 2.2		

$H_{UC}$ ,  $H_{ATRM}$  and  $H_{ATRM,CR}$  are the paleointensity values of the individual samples with associated errors for the uncorrected, ATRM corrected and ATRM and cooling rate (CR) corrected determinations, respectively.  $H_{ATRM}$  errors are calculated as minimum-maximum errors including the uncertainty of the uncorrected paleointensity  $\sigma_{UC}$  and of the ATRM correction factor  $f_{ATRM}$ .  $H_{ATRM,CR}$  errors are calculated via full error propagation using the uncertainties of  $H_{UC}$ ,  $f_{ATRM}$  and  $f_{CR}$ . Also shown are arithmetic means and standard deviations of the different sites and weighted means for the whole 8 ka flow (using  $1/(\text{arithmetic standard deviation of site means})$  as weighting parameter).

**Paleointensity on 8 ka  
New Zealand  
obsidian**

A. Ferk et al.

**Fig. 1.** Global distribution of archeomagnetic data for the last 10 ka.

Title Page

Abstract

Introduction

Conclusions

References

Tables

Figures

◀

▶

◀

▶

Back

Close

Full Screen / Esc

Printer-friendly Version

Interactive Discussion



**Paleointensity on 8 ka  
New Zealand  
obsidian**

A. Ferik et al.

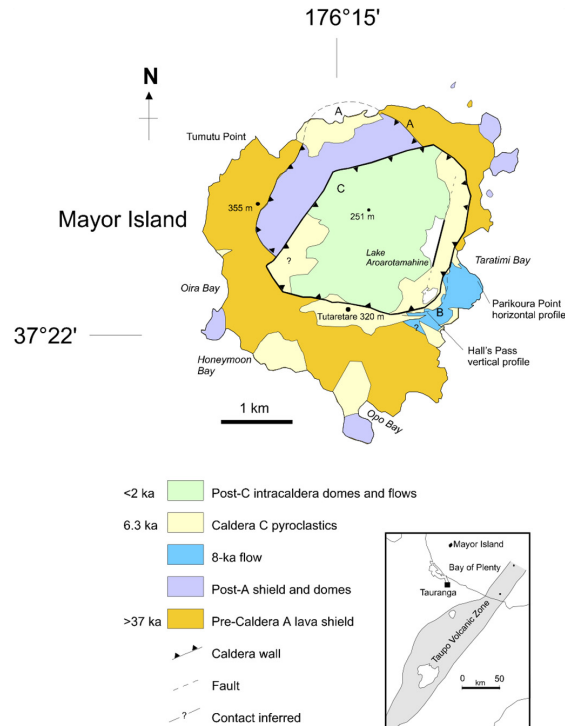


**Fig. 2.** Location of Mayor Island and geology map including the identification of caldera parts A, B and C and location of investigated sites (LOBS: Hall’s Pass, UOBS: Parikoura Point) within the 8 ka flow (blue). Taken from Gottsmann and Dingwell (2002).

Title Page

Abstract Introduction

Conclusions References

Tables Figures

◀ ▶

◀ ▶

Back Close

Full Screen / Esc

Printer-friendly Version

Interactive Discussion



---

**Paleointensity on 8 ka  
New Zealand  
obsidian**A. Ferik et al.

---

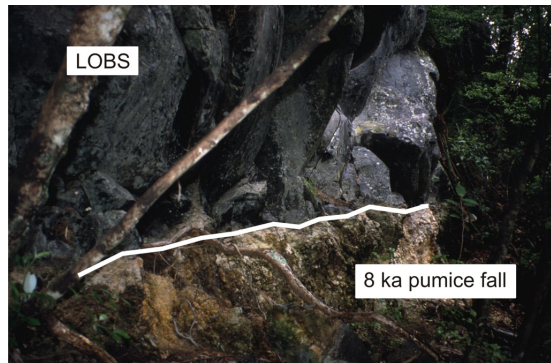


**Fig. 3.** Investigated site at Hall's Pass with LOBS (lower obsidian layer; grey to black colour) overlying the whitish 8 ka pumice fall (transition between the two indicated by white line). Taken from Gottsmann and Dingwell (2002).

[Title Page](#)[Abstract](#)[Introduction](#)[Conclusions](#)[References](#)[Tables](#)[Figures](#)[◀](#)[▶](#)[◀](#)[▶](#)[Back](#)[Close](#)[Full Screen / Esc](#)[Printer-friendly Version](#)[Interactive Discussion](#)



**Fig. 4.** Series of flow ridges of the UOBS (upper obsidian layer) at Parikoura Point. Hammer lies in the middle of a 5 m wide pinch of one flow ridge that is part of the ~30 m long investigated horizontal profile. Taken from Gottsmann and Dingwell (2002).

## SED

3, 679–711, 2011

### Paleointensity on 8 ka New Zealand obsidian

A. Ferk et al.

Title Page

Abstract

Introduction

Conclusions

References

Tables

Figures

◀

▶

◀

▶

Back

Close

Full Screen / Esc

Printer-friendly Version

Interactive Discussion



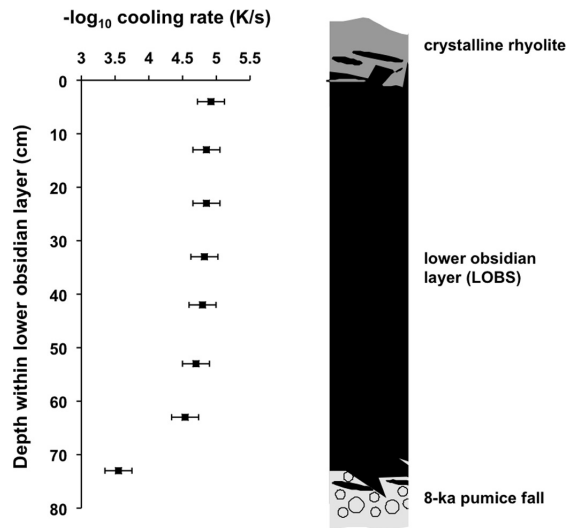


**Fig. 5.** Modelled cooling rates of LOBS as a function of profile depth. Cooling rates increase gradually towards the underlying 8 ka pumice fall. Taken from Gottsmann and Dingwell (2002).

**Paleointensity on 8 ka  
New Zealand  
obsidian**

A. Ferik et al.

Title Page

Abstract

Introduction

Conclusions

References

Tables

Figures

◀

▶

◀

▶

Back

Close

Full Screen / Esc

Printer-friendly Version

Interactive Discussion



---

**Paleointensity on 8 ka  
New Zealand  
obsidian**

A. Ferk et al.

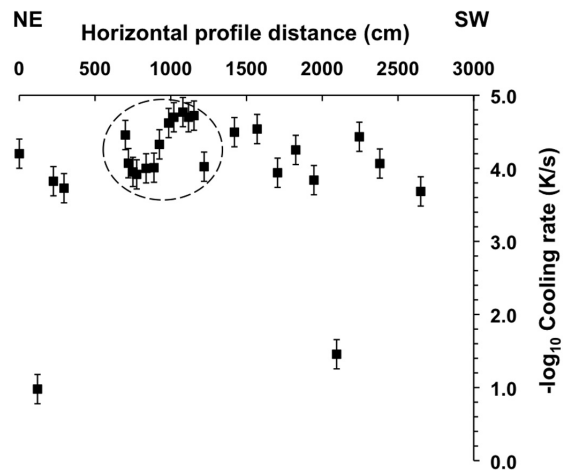


**Fig. 6.** Modelled cooling rates of UOBS as a function of horizontal profile length. Though two outliers have higher cooling rates, majority of samples shows cooling rates between  $0.01$  and  $0.001 \text{ K min}^{-1}$ . Encircled is data from one in detail analyzed 5 m long flow ridge. Taken from Gottsmann and Dingwell (2002).

[Title Page](#)[Abstract](#)[Introduction](#)[Conclusions](#)[References](#)[Tables](#)[Figures](#)[◀](#)[▶](#)[◀](#)[▶](#)[Back](#)[Close](#)[Full Screen / Esc](#)[Printer-friendly Version](#)[Interactive Discussion](#)

**Paleointensity on 8 ka  
New Zealand  
obsidian**

A. Ferik et al.

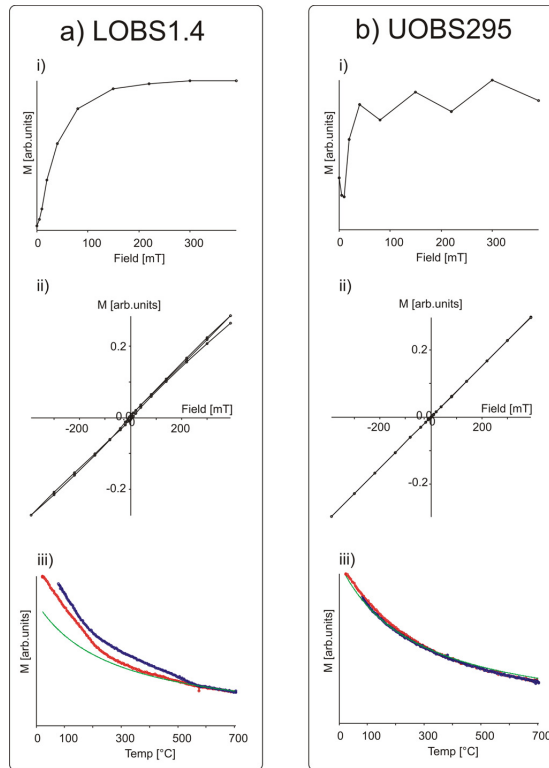


**Fig. 7.** VFTB measurements for samples **(a)** LOBS1.4 and **(b)** UOBS295: (i) IRM acquisition, (ii) hysteresis loops and (iii) thermomagnetic curves (red: heating, blue: cooling, green: paramagnetic decay).

Title Page

Abstract

Introduction

Conclusions

References

Tables

Figures

◀

▶

◀

▶

Back

Close

Full Screen / Esc

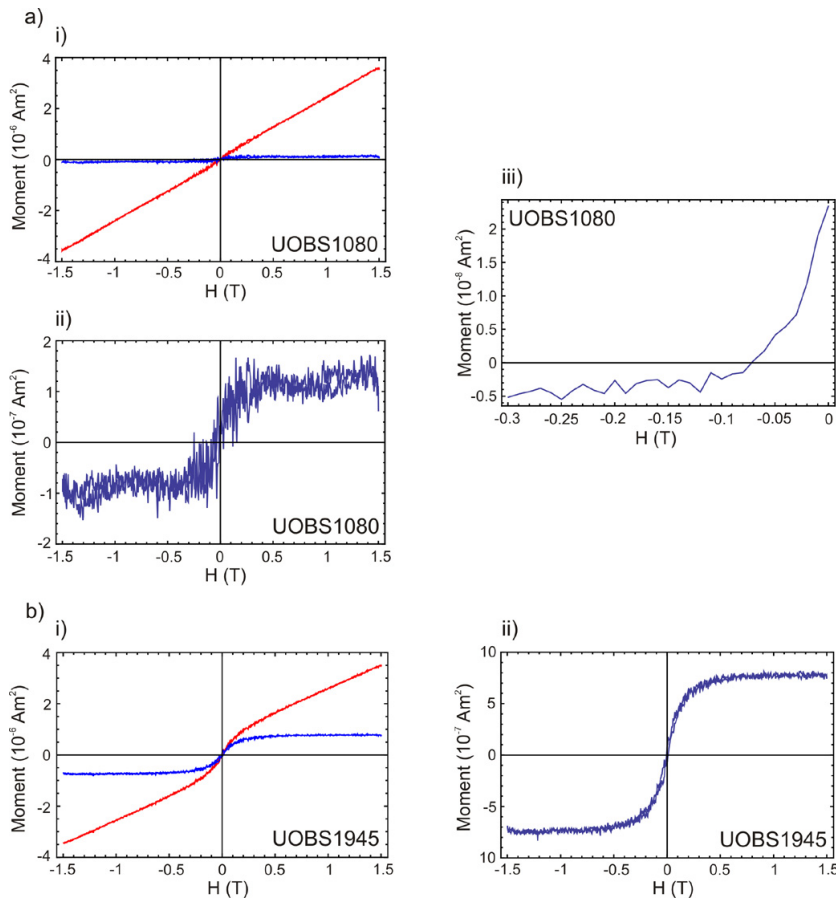
Printer-friendly Version

Interactive Discussion



## Paleointensity on 8 ka New Zealand obsidian

A. Ferik et al.

[Title Page](#)
[Abstract](#)
[Introduction](#)
[Conclusions](#)
[References](#)
[Tables](#)
[Figures](#)
[Back](#)
[Close](#)
[Full Screen / Esc](#)
[Printer-friendly Version](#)
[Interactive Discussion](#)


**Fig. 8.** VSM measurements at  $50^\circ\text{C}$  for **(a)** UOBS1080 and **(b)** UOBS1945. Graphs show (i) hysteresis loops as measured (red) and corrected for the high field slope ( $>1\text{ T}$ , blue) and (ii) the corrected loops separately in blow-ups. (iii) gives an additional backfield curve for UOBS1080.

## Paleointensity on 8 ka New Zealand obsidian

A. Ferk et al.

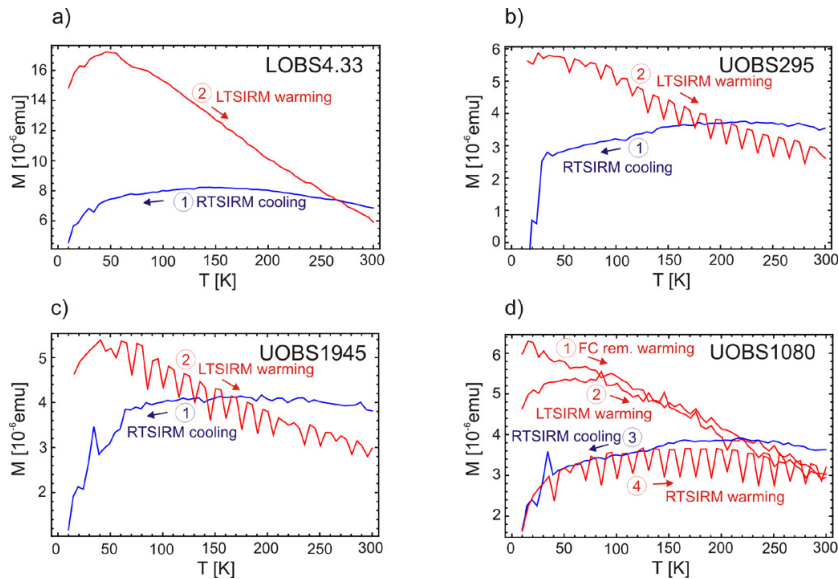


**Fig. 9.** MPMS measurements for samples **(a)** LOBS4.33, **(b)** UOBS295, **(c)** UOBS1945 and **(d)** UOBS1080. **(a)**, **(b)** and **(c)** show (1) a room temperature (RT) SIRM measured during cooling and (2) a low temperature (LT, at 10 K) SIRM measured during warming. **(d)** shows (1) a field cooled remanence measured during warming, (2) a LTSIRM measured during warming, (3) a RTSIRM measured during cooling and (4) during warming. In all cases measurements were done in zero field and applied fields for RTSIRM, LTSIRM and field cooling were 2.5 T.

Title Page

Abstract

Introduction

Conclusions

References

Tables

Figures

◀

▶

◀

▶

Back

Close

Full Screen / Esc

Printer-friendly Version

Interactive Discussion



## Paleointensity on 8 ka New Zealand obsidian

A. Ferik et al.

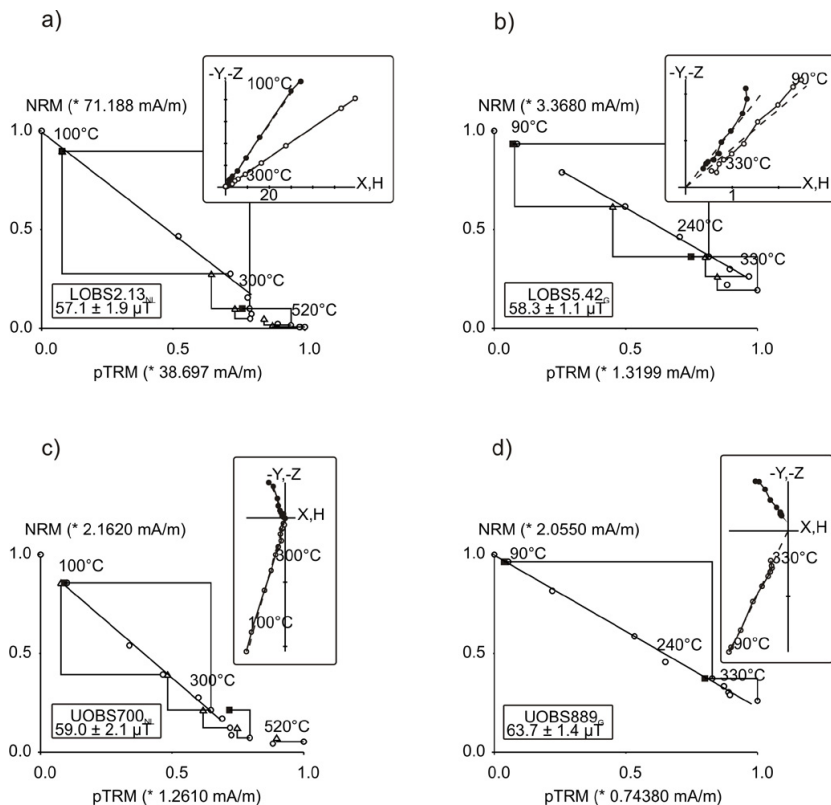


**Fig. 10.** NRM/pTRM plots and respective orthogonal projections for **(a)** LOBS2.13, **(b)** LOBS5.42, **(c)** UOBS700 and **(d)** UOBS889. Triangles and squares in the NRM/pTRM plots indicate pTRM checks (CK) and additivity checks (AC), respectively.

[Title Page](#)
[Abstract](#)
[Introduction](#)
[Conclusions](#)
[References](#)
[Tables](#)
[Figures](#)
[◀](#)
[▶](#)
[◀](#)
[▶](#)
[Back](#)
[Close](#)
[Full Screen / Esc](#)
[Printer-friendly Version](#)
[Interactive Discussion](#)

## Paleointensity on 8 ka New Zealand obsidian

A. Ferk et al.

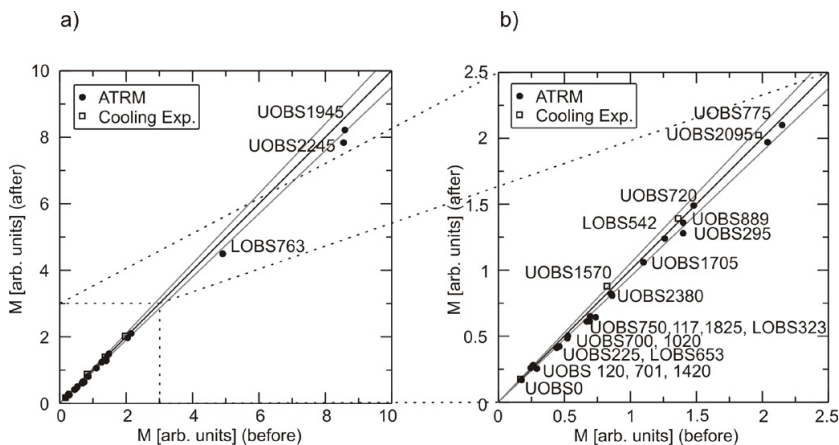


**Fig. 11.** Comparison of magnetization before and after the ATRM (filled circle) and cooling rate (open square) experiments. Diagonal in the plots represents no alteration and grey cone around this line gives 5% deviation between the two measurements. **(b)** shows close-up of lower left corner of **(a)**.

Title Page

Abstract

Introduction

Conclusions

References

Tables

Figures

◀

▶

◀

▶

Back

Close

Full Screen / Esc

Printer-friendly Version

Interactive Discussion

